11th Australasian Fluid Mechanics Conference
University of Tasmania, Hobart, Australia
14-18 December 1992

THE EFFECTS OF FREE SURFACE AND RIGID BOUNDARY ON A VAPOUR CAVITY BUBBLE

Ching-fu YU and Wee King SOH

Department of Mechanical Engineering, University of Wollongong
Locked Bag 8844, South Coast Mail Centre, NSW 2521, AUSTRALIA

ABSTRACT

The experimental studies of the evolution of a vapour cavity bubble have shown many interesting characteristics. This paper mainly investigates the situation in which the bubble lies between free surface and a horizontal rigid wall. By varying the depth of the water, various magnitudes of interference from the free surface and the rigid boundary can be regulated.

Observations show that the vortex ring follows the formation of the micro-jet. For this phenomenon to occur it requires the Bjerknes forces induced from both the rigid boundary and the free surface. In addition, both the vortex ring and the micro-jet will only have time to develop if the elapse time for the evolution of the bubble is within a certain threshold. The ability for the vapour cavity bubble to bring damage to the nearby surface is discussed in the light of these results.

INTRODUCTION

The behaviour of a cavity bubble, which expands to a maximum radius and then collapses under the influence of the dynamic instability, is an important factor to the damage or erosion of hydrodynamic machines. There is a peak pressure while the bubble collapses near a solid wall (Kimoto et al., 1987). When the cavity is near a free surface, a spike shape of free surface develops before the expansion of cavity bubble concludes (Blake and Gibson, 1981).

In the past, most studies concerning the mechanism of cavity bubble's dynamics were concentrated on a cavity bubble near either the free surface (Chahine, 1977; Blake and Gibson, 1981; and Blake et al., 1987) or the rigid boundary (Cerone and Blake, 1983; Shima et al., 1983; Kimoto et al., 1985; Blake et al., 1986; Tomita and Shima, 1986; Blake and Gibson, 1987; Nienaltowska, 1989; and Vogel et al., 1989). They considered only "small bubbles" (maximum radius of bubbles below 5 mm). In the case of bubbles generated by an underwater explosion, the effects of both rigid boundary and free surface are presented. The present study is to investigate the behaviour of a cavity bubble under both effects of free surface and rigid boundary by applying a spark discharge technique and high-speed photography. The volume of the bubble is greater than that of the early studies in order to obtain a significant buoyancy effect. Various magnitudes of interference from the free surface and the rigid boundary are regulated by using a fixed distance of cavity bubble to the rigid boundary and varying the depth of water, as shown in Figure 1. For the cases of varying the distance of a cavity to the rigid boundary and fixed depth of water will not be considered here.

EXPERIMENTS

Figure 2 shows the schematic diagram of the present cavity bubble's experimental apparatus. It is similar to the rig developed by Benjamin and Ellis (1966) and Gibson (1968).

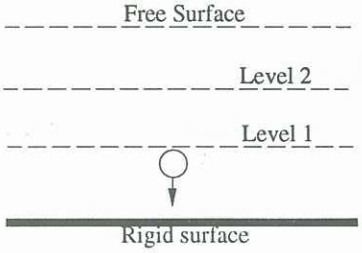

Figure 1 Bubble behaviour under the effects of free surface and rigid boundary.

A spark discharge technique is used to generate a vapour cavity underwater. Only a single bubble will be produced in each experiment.

The cavity tank was made by using 10 mm thick perspex glass with an internal diameter of 260 mm and a depth of 370 mm. In order to record the evolution of a cavity bubble properly, a flat perspex is used as a window in the cylinder tank. The thickness of the window in the cylindrical tank is 25 mm. The depth of the tap water in the small cavity tank varies from 45mm to 185 mm. In the bottom of the tank, there is a perspex rigid boundary.

The tungsten electrodes, which transmit high voltage current are submerged in the water of cavity tank. The gap of the electrodes is normally 0.5 mm. After a few runs of the experiment, the gap will be widen and required re-adjustment. In order to increase the period of first pulsation and degas the water suggested by Chahine (1977), a vacuum pump is used to lower the ambient pressure to about 7 kPA in the cavity tank.

A NAC high speed cine-camera model E-10, which has the ability to record up to 10,000 FPS (frame per second), is used to capture the motion of the bubbles. The present experiment employed the framing rate of 6000 FPS. The lens of the camera is Micro-Nikkor 55 mm f/2.8. The film type is black and white, reversal Kodak Tri-x 30.2 m. In the experiment the event occurred almost instantly (i.e. 14 milliseconds), therefore the camera was set in pre-start mode. When the high speed camera reaches required high speed, it will send an electrical pulse from its relay circuit to the thyratron which in turn will trigger a spark instantly. A synchronous circuit was made. After reaching the required camera speed, the synchronous circuit transmits a signal to cavitation circuit to generate a spark.

The present experimental conditions:
Energy input: 0.25 mF @ 10 kV
The distance of electrodes to the rigid boundary, h=35 mm.
Water level (mm)= 45, 60, 75, 90, 105, 120, 135, 150, 165, and 180 mm.
The pressure difference between the ambient pressure and vapour pressure, Δp, = 7 kPa.

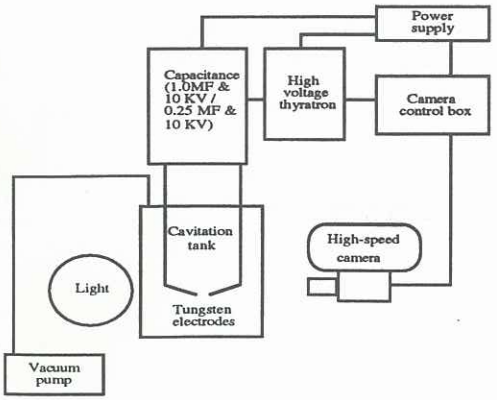

Figure 2 Schematic diagram of the explosion bubble's experimental arrangement.

RESULTS

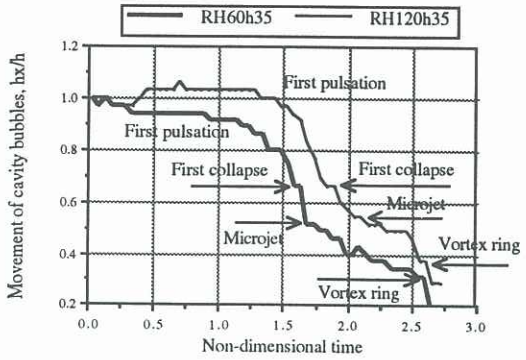

Figure 3 The migration of cavity bubbles generated at fixed location and different water levels.

Figure 3 shows the migration of cavity bubbles generated at a fixed distance, h=35 mm, from the rigid boundary, and different water level, H= 60 mm, and 120 mm. The evolution of the cavity bubbles for both cases are similar: A microjet appears after the first pulsation. Following the microjet, a vortex ring forms before the cavity bubble collides with the rigid boundary. For a given value of h (=35 mm), the closer the free surface to the bubble, the formation of microjet will be sooner after the formation of the bubble. This depicts the influence of the repelling force induced by the free surface.

Table I lists the maximum bubble radius and the observations in reference to vortex rings at different water levels. It is interesting to note that the vortex ring always occurs while the water level, H, in the range of 4 Rmax<H<8 Rmax (Rmax= maximum radius of a cavity). No vortex ring exists in the case of RH45h35 and RH75h35. The reasons are (i) the bubble size is too large and there is not enough space for a vortex ring to evolve and (ii) the combined forces caused by both free surface and rigid boundary are so strong that the bubble collides with the rigid boundary and there is no time available for a vortex ring to form.

As the water level gradually increases, the effect of free surface decreases correspondingly. Since the distance of bubble to the rigid boundary, h, is being held constant, the effect of rigid boundary completely depends upon the size of the cavity bubble. For the cases of RH165h35 and RH180h35, where the effect of free surface on these cases can be neglected due to the distance of bubble to free surface is over 7 times of maximum bubble radius, there is no vortex ring generated.

Table I. The relationship of vortex ring, water level, and bubble size

Exp. No.	Water level , H (mm)	Rmax (mm)	Observations
RH45h35	45	20.0	No vortex ring
RH60h35	60	17.5	Vortex ring
RH75h35	75	19.0	No vortex ring
RH90h35	90	18.5	Vortex ring
RH105h35	105	18.0	Vortex ring
RH120h35	120	17.0	Vortex ring
RH135h35	135	18.0	Vortex ring
RH150h35	150	18.5	Vortex ring
RH165h35	165	15.0	No vortex ring
RH180h35	180	20.5	No vortex ring

In general, the cavity bubble expands spherically, and moves downwards in the collapse stage of first pulsation. During the re-expansion, both upper and lower surface of cavity bubble, under both repelling force contributed by the free surface and attraction by the rigid boundary, move faster than the side of the bubble. Therefore, the upper surface penetrates into the bubble and through to the lower surface. A leading jet is formed and directs downwards. Lauterborn (1982) described the above phenomenon and explained that the highly curved parts of a cavity bubble, i.e. the top and bottom of a bubble, collapse faster than less curved parts. The vortex ring appears during the collapse stage of second pulsation. Figure 4 shows the shape of cavity bubble at this re-expansion stage. Following the re-expansion, the upper surface completely passes through the side part of the bubble and forms a faster moving "separate" bubble below the original one. At the same time, the curved side of the bubble forms a vortex ring due to its slow movement. Figure 5 shows a conceptual diagram of the shape of cavity bubble when the vortex ring appears.

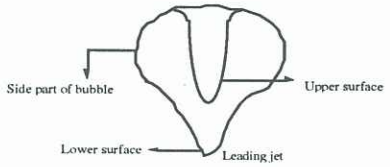

Figure 4 The shape of cavity bubble during the re-expansion stage.

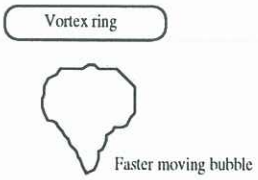

Figure 5 The shape of cavity bubble while the vortex ring appears.

Table II lists the non-dimensional position and buoyancy parameters of the experimental results, (i.e. γ, δ) and the period of the first pulsation $T_c{}^{1*}$. The values of δ is made constant (=0.16). It is interesting to note that the period of the first pulsation increases with the increasing water depth. The trend of the non-dimensional period for the present study shows that the effect of free surface decreases gradually with the increasing water depth. It means that the repelled force from the free surface gradually decreases with the increasing water depth, leaving only the attraction from the rigid boundary to act on the bubble.

Table II. Non-dimensional parameters of the experimental results

Experimental No.	γ	δ	T_c^{1*}
RH45h35	1.75	0.17	1.43
RH60h35	2.00	0.16	1.54
RH75h35	1.84	0.16	1.65
RH90h35	1.89	0.16	1.65
RH105h35	1.94	0.16	1.64
RH120h35	2.06	0.15	1.74
RH135h35	1.94	0.16	1.69
RH150h35	1.89	0.16	1.74
RH165h35	2.33	0.15	1.85
RH180h35	1.71	0.17	2.00

where

$$\gamma = \frac{h}{R_{max}}, \quad \delta = \sqrt{\frac{\rho g R_{max}}{\Delta p}},$$

T_c^{1*} = Non-dimensional period of the first pulsation;

$$T_c^{1*} = t\sqrt{\frac{\Delta p}{R_{max}}};$$

R_{max} = the maximum radius of bubbles,
h = the distance of the electrodes to the rigid boundary,
Δp = the pressure difference between the ambient pressure and the vapour pressure,
ρ = the density of the liquid,
t = time (sec)

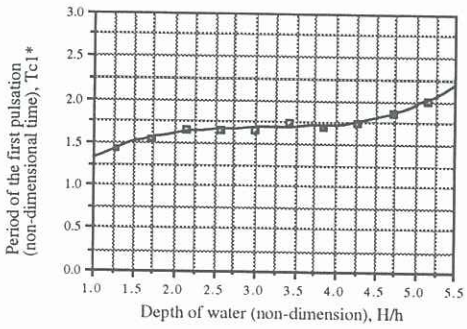

Figure 6 The relationship of the period of first pulsation, T_c^{1*}, with the depth of water, (H/h).

Figure 6 shows the relationship of the period of the first pulsation, T_c^{1*}, with the depth of water (H/h). Evidently the period of the first pulsation, T_c^{1*}, increases slightly with the increasing depth of water (H/h). This phenomenon can be explained by the combination of the buoyancy and the repelling force of free surface. The repelling force gradually decreases with the increasing water depth. Under this situation, the buoyancy explicitly plays an important role and causes the period of the first pulsation to increase.

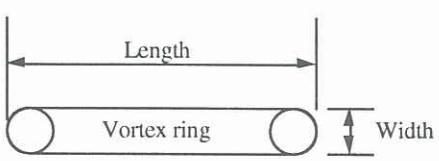

Figure 7 Schematic diagram of a vortex ring's original size

Figure 7 shows the schematic diagram of a vortex ring's original size. The migration of the ring directs to the rigid boundary. The dimensions of the initial vortex ring are expressed by length (L) and width (W), as shown in Table III. Compared with the results of Vogel, Lauterborn and Timm (1989), the velocities of the present vortex rings are only half velocity of their vortex rings. In two cases of their vortex ring, they reported that the velocities are 6.4 m/sec and 5.2 m/sec; and indicated that the smaller velocity results from the smaller size of the bubble involved. Evidently, the size of their laser-generated cavity bubbles are smaller than that of the present spark-generated bubbles. The maximum radius of bubbles in the present study are about 17.0-18.5 mm. However, the velocity of a vortex ring is not only dependent on the size of a cavity bubble, but also on other factors, such as the strength of vorticity, its initial location and its initial diameter. The trajectories of the vortex rings are shown in Figure 8.

Table III The size and velocities of the initial vortex rings

Exp. No.	W (mm)	L (mm)	h_{Ring} (mm)	Rmax (mm)	V (m/sec)
RH60h35	2.5	13.0	15.0	17.5	2.79
RH90h35	4.0	16.0	12.0	18.5	3.15
RH105h35	3.0	12.0	18.0	18.0	3.66
RH120h35	4.0	10.0	18.0	17.0	3.20
RH135h35	3.0	12.0	15.0	18.0	3.09
RH150h35	4.0	13.0	15.0	18.5	3.26

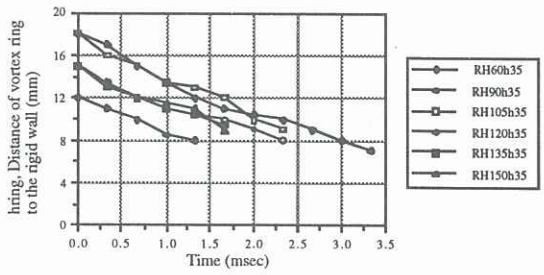

Figure 8 The movement of the vortex rings

Table IV shows the locations of the initial microjet γ_j (= h_j/R_{max}, and h_j is the distance of the rigid boundary to the bubble centroid in which the microjet was first observed) and vortex ring γ_v (= h_v/R_{max}, and h_v is the distance of the rigid boundary to the bubble centroid in which the vortex ring was first observed). It indicates that a necessary condition for the occurrence of vortex rings is for the location of initial microjet to be greater than 0.50. Figure 9 shows the evolution of a cavity bubble when water level, H=45 mm, and h=35 mm. For this case the location of initial microjet is 0.34 and thus no vortex ring occurs. The location for the initial vortex ring is within 0.34 - 0.51.

Table IV The locations of the initial microjet & vortex ring

Exp. No.	Location of initial vortex ring (γ_v)	Location of initial microjet (γ_j)
RH60h35	0.43	0.52
RH90h35	0.34	0.68
RH105h35	0.51	0.67
RH120h35	0.51	0.54
RH135h35	0.43	0.50
RH150h35	0.43	0.60

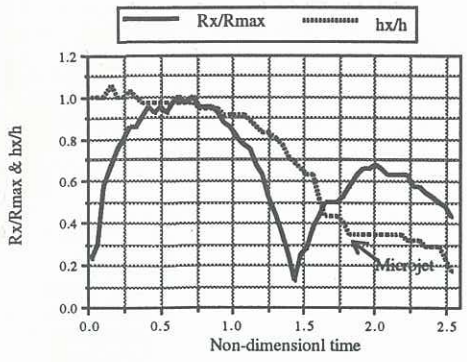

Figure 9 The evolution of a cavity bubble when water level, H=45 mm, and h=35 mm.

CONCLUSIONS

The behaviour of a cavity bubble under the effects of free surface and rigid boundary has been investigated experimentally using a spark discharge technique to generate the bubble and high-speed photography for recording. Using the fixed distance, h, of a cavity bubble to the rigid boundary and varying the water depth, H, it reveals that there are two significant water levels: H= 4 Rmax and H=8 Rmax. Within these two levels, under both effects of the free surface and rigid boundary a distinguished vortex ring following the microjet appears in the second pulsation. It is found that the range of the non-dimensional parameters γ and δ for the occurrence of a vortex ring are 1.89-2.06 and 0.15-0.16, respectively. It is in agreement with the observation of Vogel et al (1989) by using laser-produced cavity bubbles. The initial location of the microjet plays an important role for the occurrence of vortex ring.

For H below 4 Rmax, there is a strong influence from the free surface on the evolution of a cavity bubble. The cavity bubble, under the combined forces from the free surface and rigid boundary, moves quickly downward and collides on the rigid boundary. A microjet appears in the expansion stage of second pulsation and directs downward. Since the microjet is much nearer to the rigid boundary than that of other cases, i.e. the location of the microjet is 0.34 γ, no vortex ring can be observed.

For H above 8 Rmax, the effect of the free surface on the cavity bubble can be neglected due to the large distance between the bubble and the free surface.

ACKNOWLEDGEMENT

The present work was supported by the Material Research Lab. of the Australia Defence Science and Technology Research.

REFERENCES

BENJAMIN, T.B. and ELLIS, A.T. (1966) The Collpase of Cavitation Bubbles and the Pressure thereby Produced against Solid Boundaries. Phil. Trans. Roy. Soc. A260, 221-240.

BLAKE J R and GIBSON, D C (1981) Growth and Collapse of a Vapour cavity near a Free Surface. Journal of Fluid Mechanics, 111, 123-140.

BLAKE, J R, and GIBSON, D C (1987) Cavitation Bubbles near Boundaries. Ann. Rev. Fluid Mech., 19, 99-123.

BLAKE, J R, TAIB, B B, and DOHERTY, G (1986) Transient Cavities near Boundaries Part 1. Rigid Boundary. Journal of Fluid Mechanics, 170, 479-497.

BLAKE, J R , TAIB, B B , and Doherty, G (1987) Transient Cavities near Boundaries, Part 2. Free Surface. Journal of Fluid Mechanics, 181,197-212.

CERONE, P. and BLAKE, J R (1984) A Note on the Instantaneous Streamlines, Pathlines and Pressure Contours for a Cavitation Bubble Near a Boundary. Journal of Australia Math. Soc. Ser. B 26, 31-44.

CHAHINE, G L (1977) Interaction Between an Oscillating Bubble and a Free Surface. Journal of Fluids Engineering, 709-716.

GIBSON, D.C. (1968) Cavitation Adjacent to Plane Boundaries. In Proc. 3rd Aust. Conf. on Hydraulics and Fluid Mechanics, 210-214.

KIMOTO, H, KAMOTO, A, HIROSE, T and YOSHINOBU, H (1987) A Study on Impulsive Pressure of a Collapsing Cavitation Bubble. JSME International Journal, 30 (261), 449-457.

KIMOTO, H, MOMOSE, K, UEKI, H and ONISHI, T (1985) A Study of a Cavitation Bubble on a Solid Boundary. Bulletin of JSME, 28 (238), 601-609.

NIENALTOWSKA, E (1989) The Use of a Photoelastic Method to Study the Effects of Bubble Collapse on Surfaces. Journal of Fluids Engineering, 111, 353-356.

SHIMA, A, TAKAYAMA, K, TOMITA, Y, and OHSAWA, N (1983) Mechanism of Impact Pressure Generation from Spark-Generation Bubble Collapse Near a Wall. AIAA Journal, 21, (1), 55-59.

TOMITA, Y and SHIMA, A (1986) Mechanisms of Impulsive Pressure Generation and Damage Pit Formation by Bubble Collapse. Journal of Fluid Mechanics, 169, 535-564.

VOGEL, A, LAUTERBORN, W, and TIMM, R (1989) Optical and Acoustic Investigations of the Dynamics of Laser-Produced Cavitation Bubbles near a Solid Boundary. Journal of Fluid Mechanics, 206, 299-338.